JVST B
Journal of Vacuum Science & Technology B

Electrical characterization of InGaAs ultra-shallow junctions

Cite as: J. Vac. Sci. Technol. B **28**, C1C41 (2010); https://doi.org/10.1116/1.3231492
Submitted: 11 June 2009 . Accepted: 24 August 2009 . Published Online: 01 March 2010

Dirch H. Petersen, Ole Hansen, Peter Bøggild, Rong Lin, Peter F. Nielsen, Dennis Lin, Christoph Adelmann, Alireza Alian, Clement Merckling, Julien Penaud, Guy Brammertz, Jozefien Goossens, Wilfried Vandervorst, and Trudo Clarysse

View Online

Export Citation

ARTICLES YOU MAY BE INTERESTED IN

Review of electrical characterization of ultra-shallow junctions with micro four-point probes
Journal of Vacuum Science & Technology B **28**, C1C27 (2010); https://doi.org/10.1116/1.3224898

Sensitivity study of micro four-point probe measurements on small samples
Journal of Vacuum Science & Technology B **28**, C1C34 (2010); https://doi.org/10.1116/1.3224889

Accurate microfour-point probe sheet resistance measurements on small samples
Review of Scientific Instruments **80**, 053902 (2009); https://doi.org/10.1063/1.3125050

HIDEN ANALYTICAL
Instruments for Advanced Science
Contact Hiden Analytical for further details:
W www.HidenAnalytical.com
E info@hiden.co.uk
CLICK TO VIEW our product catalogue

Gas Analysis
dynamic measurement of reaction gas streams
catalysis and thermal analysis
molecular beam studies
dissolved species probes
fermentation, environmental and ecological studies

Surface Science
UHV TPD
SIMS
end point detection in ion beam etch
elemental imaging - surface mapping

Plasma Diagnostics
plasma source characterization
etch and deposition process reaction kinetic studies
analysis of neutral and radical species

Vacuum Analysis
partial pressure measurement and control of process gases
reactive sputter process control
vacuum diagnostics
vacuum coating process monitoring

© 2009 American Vacuum Society.

Electrical characterization of InGaAs ultra-shallow junctions

Dirch H. Petersen[a)]
Department of Micro- and Nanotechnology, Technical University of Denmark, DTU Nanotech, Building 345 East, DK-2800 Kgs. Lyngby, Denmark; CAPRES A/S, Scion-DTU, Building 373, DK-2800 Kgs. Lyngby, Denmark; and IMEC, Kapeldreef 75, B-3001 Leuven, Belgium

Ole Hansen
Department of Micro- and Nanotechnology, Technical University of Denmark, DTU Nanotech, Building 345 East, DK-2800 Kgs. Lyngby, Denmark and Centre for Individual Nanoparticle Functionality (CINF), Technical University of Denmark, Building 345 East, DK-2800 Kgs. Lyngby, Denmark

Peter Bøggild
Department of Micro- and Nanotechnology, Technical University of Denmark, DTU Nanotech, Building 345 East, DK-2800 Kgs. Lyngby Denmark

Rong Lin and Peter F. Nielsen
CAPRES A/S, Scion-DTU, Building 373, DK-2800 Kgs. Lyngby, Denmark

Dennis Lin, Christoph Adelmann, Alireza Alian, and Clement Merckling
IMEC, Kapeldreef 75, B-3001 Leuven, Belgium

Julien Penaud
Riber, rue Casimir Perier 31, 95870 Bezons Cedex, France

Guy Brammertz and Jozefien Goossens
IMEC, Kapeldreef 75, B-3001 Leuven, Belgium

Wilfried Vandervorst
IMEC, Kapeldreef 75, B-3001 Leuven, Belgium and Inst. voor Kern-en Stralingsfysica, K. U. Leuven, Celestijnenlaan 200D, B-3001 Leuven, Belgium

Trudo Clarysse
IMEC, Kapeldreef 75, B-3001 Leuven, Belgium

(Received 11 June 2009; accepted 24 August 2009; published 1 March 2010)

In this study, we investigate the limitations to sheet resistance and Hall effect characterization of ultra-shallow junctions (USJs) in $In_{0.53}Ga_{0.47}As$. We compare conventional van der Pauw and Hall effect measurements with micro four-point probe (M4PP) and micro Hall effect methods. Due to the high carrier mobility of InGaAs, we extend the micro-Hall effect position error suppression method to also take geometrical magnetoresistance into account. We find that the conventional techniques fail to measure accurately on n^{++}/p^{+} USJ due to a significant leakage current, whereas the M4PP and micro Hall effect methods are able to give accurate results. Finally, we observe a significant reduction in the carrier mobility for InGaAs USJ. © *2009 American Vacuum Society.*
[DOI: 10.1116/1.3231492]

I. INTRODUCTION

High mobility substrate materials, such as InGaAs and Ge, have attracted much attention in recent post Si-CMOS device research device. In order to continue device scaling beyond the 22 nm technology node, it is crucial to obtain heavily doped source/drain regions and abrupt junctions in these high mobility semiconductor materials. The study of ultra-shallow implants in InGaAs could ultimately answer questions of scalability associated with such devices, and thus indicate the potential for the development of high performance electronics. Conventional semiconductor metrology methods are, however, often inadequate in characterizing nanoscale materials as these are not specifically designed for structures with extreme dimensions.

It has previously been demonstrated that sheet resistance characterization of ultra-shallow junctions (USJs) in Si with conventional four-point probes is highly unreliable.[1] In contrast, micro four-point probes (M4PPs) are able to accurately characterize sub-10-nm junctions with zero probe penetration, which both reduce sample damage and provide more reliable measurements. Since InGaAs is much softer than Si, one would expect probe penetration to be more pronounced and sheet resistance measurements on ultra-shallow junctions become even more difficult. In addition to sheet resistance characterization, it was recently demonstrated that micro Hall effect measurements can be performed with M4PP in proximity of an insulating barrier.[2] By using a position error suppression technique, in combination with the micro Hall effect method, the measurement accuracy could be improved, while the measurement time was reduced to less than a minute.[3] However, a combination of a very high

[a)]Electronic mail: dhpe@nanotech.dtu.dk

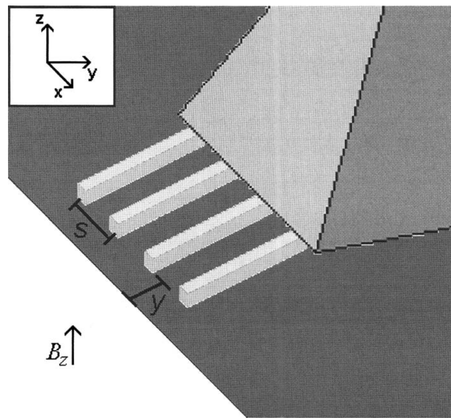

FIG. 1. Schematic illustration of a M4PP measuring close to the edge of a cleaved wafer.

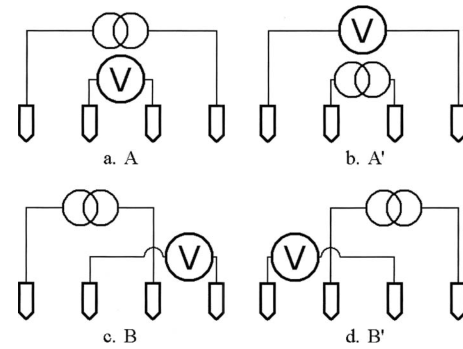

FIG. 2. Illustration of the four electrode combinations A, A′, B, and B′, which are used in micro Hall effect measurements. Adapted from Ref. 3.

carrier mobility and a moderate magnetic flux density may affect the result of micro Hall effect measurement with position error suppression because of a geometrical magnetoresistive contribution.[4]

In this article, we extend the position error suppression method to allow for micro Hall effect measurements in the presence of a geometrical magnetoresistance contribution. We then study sheet resistance and Hall effect characterization of highly doped $In_{0.53}Ga_{0.47}As$ by conventional van der Pauw (VDP) and Hall effect measurements on square test samples and compare to M4PP and micro Hall effect measurements. Finally, we investigate both ion implanted InGaAs and *in-situ* doped epitaxially grown layers with layer thicknesses down to 19 nm.

II. MICRO HALL EFFECT THEORY

Hall effect measurements may be performed on a thin conductive sheet with a four-point probe placed in proximity of at least one laterally insulating boundary.[2] We will describe only the situation where a collinear equidistant four-point probe with electrode pitch s is placed on a conductive sheet at a distance y from an insulating boundary, which is parallel to the four electrode contacts (cf. Fig. 1).

The four-point resistance, $R=V/I_0$, is measured by passing a current, I_0, between two of the electrodes while the voltage difference, V, is measured between the two remaining electrodes. For the analysis of Hall effect measurements, four different electrode combinations defined as configurations A, A′, B and B′ will be used (cf. Fig. 2). With the subscript denoting the electrode configuration, we define the resistance averages, $\overline{R_{AA'}}\equiv(R_A+R_{A'})/2$ and $\overline{R_{BB'}}\equiv(R_B+R_{B'})/2$, and the resistance difference, $\Delta R_{BB'}\equiv R_B-R_{B'}$. The basic equations describing such measurements are summarized in Table I.[2,3]

For the equations in Table I, the Hall sheet resistance, $R_H=Z\mu_H B_z R_0$, is a function of the direct sheet resistance R_0, the magnetic flux density B_z, the Hall carrier mobility μ_H, and the carrier type, $Z=\pm1$. The Hall sheet resistance may also yield the Hall sheet carrier density as $N_{HS}=ZB_z/(eR_H)$, where e is the unit charge. The pseudo sheet resistance R_P extracted from the dual configuration equation is a function of R_0, R_H, and y; this will be described more detailed in the next section. The subscripts 1 and 2 refer to measurements at two different locations separated by the known distance Δy. The term $R_H^2/R_0^2=\mu_H^2B_z^2$ is due to the geometrical magnetoresistance.[4]

A. Position error suppression with magnetoresistance

We previously showed how a micro Hall effect measurement can be performed with high precision in less than a minute using a position error suppression method[3] based on four-point measurements at two locations. In this study, one measurement combining data from all four configurations is performed at a location y_1 close to the insulating boundary (the exact position is unknown). At another location, y_2, far from the boundary a second measurement is performed (e.g., for a 20 μm pitch probe, $y_1\approx4$ μm, $y_2=y_1+\Delta y$, and $\Delta y=56$ μm). However, the basic equations described previously[3] do not include the geometrical magnetoresistive contribution, which can become relevant for characterization of high mobility materials. Thus, here we show how the position error suppression method can be extended to take this contribution into account.

The solution to the pseudo sheet resistance function R_P can be found for a known magnetoresistance contribution by numeric calculation using the dual configuration equation (cf. Table I). In Fig. 3 we show the pseudo sheet resistance normalized to the direct sheet resistance R_0 for different magnetoresistance contributions. As it was previously shown for single configuration measurements,[2] it is seen that there is no geometrical magnetoresistance when the four-point probe is placed exactly at the boundary. However, since the carrier mobility is not known prior to measurement, it could be of value to have an analytical approximation to simplify the data treatment. We now demonstrate how such an approximation may be obtained.

The resistance average functions (cf. Table I) can be rewritten as dependent on two geometrical functions $f_i(y/s)$ and $g_i(y/s)$, where i denotes the configurations AA′ and BB′.

TABLE I. Basic equations describing four-point measurements on a conductive sheet with one insulating boundary parallel to the line of the four contacts (Refs. 2 and 3).

Resistance average for configuration A and A′	$\overline{R_{AA'}}=\frac{R_0}{2\pi}\left(1+\frac{R_H^2}{R_0^2}\right)\ln(4)+\frac{R_0}{2\pi}\left(1-\frac{R_H^2}{R_0^2}\right)\ln\frac{4+4\left(\frac{y}{s}\right)^2}{1+4\left(\frac{y}{s}\right)^2}$
Resistance average for configuration B and B′	$\overline{R_{BB'}}=\frac{R_0}{2\pi}\left(1+\frac{R_H^2}{R_0^2}\right)\ln(3)+\frac{R_0}{2\pi}\left(1-\frac{R_H^2}{R_0^2}\right)\ln\sqrt{\frac{9+4\left(\frac{y}{s}\right)^2}{1+4\left(\frac{y}{s}\right)^2}}$
Resistance difference for configuration B and B′	$\Delta R_{BB'}=\frac{2R_H}{\pi}\left(3\arctan\left(\frac{s}{2y}\right)-\arctan\left(\frac{3s}{2y}\right)\right)$
Dual configuration equation	$\exp\left(\frac{2\pi\overline{R_{AA'}}}{R_P}\right)-\exp\left(\frac{2\pi\overline{R_{BB'}}}{R_P}\right)=1$
Position error suppression	$f\left(\frac{y_1}{s}\right)=\frac{R_{P1}}{R_{P2}}f\left(\frac{y_1+\Delta y}{s}\right)$

$$\overline{R_{AA'}}=R_0\left(f_{AA'}(y/s)+\frac{R_H^2}{R_0^2}g_{AA'}(y/s)\right), \tag{1}$$

$$\overline{R_{BB'}}=R_0\left(f_{BB'}(y/s)+\frac{R_H^2}{R_0^2}g_{BB'}(y/s)\right). \tag{2}$$

Furthermore, it can be shown that the geometrical functions are not independent,

$$g_i(y/s)=f_i(0)-f_i(y/s). \tag{3}$$

We may expect that the pseudo sheet resistance can also be expressed in a similar manner as Eqs. (1) and (2) to a good approximation,

$$R_{P,\text{appr}}\approx R_0\left(f_P(y/s)+\frac{R_H^2}{R_0^2}g_P(y/s)\right). \tag{4}$$

In analogy to Eq. (3), we guess that $g_P(y/s)\approx f_P(0)-f_P(y/s)=2-f_P(y/s)$. Thus, the pseudo sheet resistance is, by this approximation, a simple function of the already known numerically determined function, $f_P(y/s)$,[3] and the magnetoresistive contribution. The error of the approximated pseudo sheet resistance function is shown in Fig. 4 where the relative error is calculated as $(R_{P,\text{appr}}-R_P)/R_P$ for different magnetoresistance contributions. The error initially increases with increasing magnetoresistance and returns to zero again at $\mu_H^2B_z^2=1$. However, the position error suppression method relies on measurements at two locations, e.g., at $y_1=0.2s$ and $y_2=3s$, and at these locations the relative error is quite small and acceptable.

III. EXPERIMENT

Three types of Si doped $In_{0.53}Ga_{0.47}As$ samples have been investigated. For all samples, a 1 µm thick $In_{0.53}Ga_{0.47}As$ thin film was grown epitaxially on lattice matched InP semi-insulating substrates by molecular beam epitaxy. Type IA and IB samples were doped by ion implantation (Si, 50 keV)

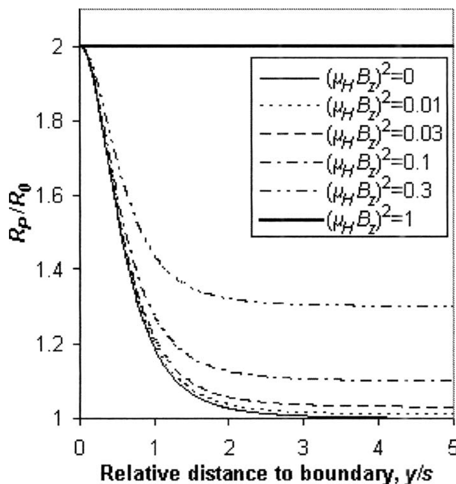

FIG. 3. Pseudo sheet resistance normalized to the direct sheet resistance with different contributions to the geometrical magnetoresistance.

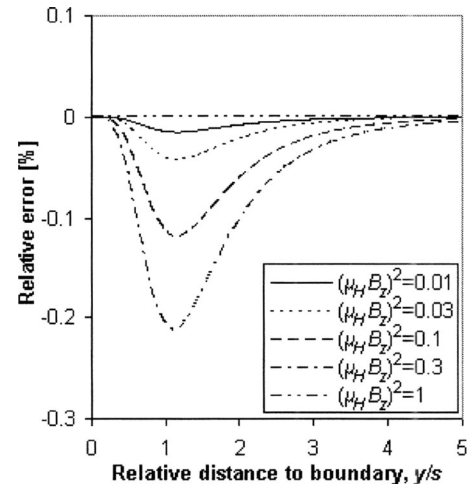

FIG. 4. Relative error of the pseudo sheet resistance approximation for different contributions to the geometrical magnetoresistance.

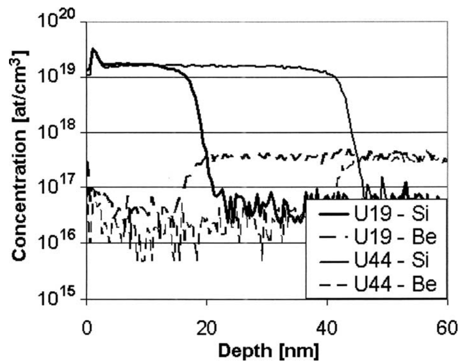

FIG. 5. Dopant concentration of the U19 and U44 samples measured using SIMS.

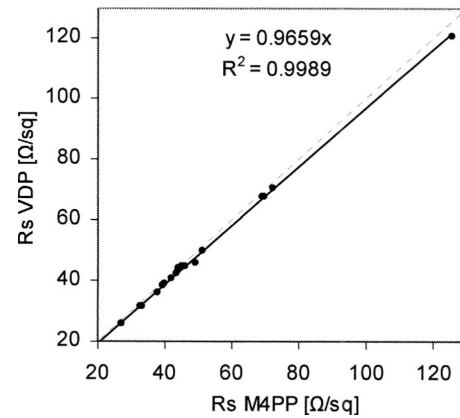

FIG. 7. Comparison of sheet resistance measured using VDP and M4PP, respectively. The samples measured were $In_{0.53}Ga_{0.47}As$ doped with 10^{14} and 10^{15} atoms/cm^2 Si implanted at 50 keV.

with nominal doses of 10^{14} and 10^{15} cm^{-2}, respectively, followed by annealing at different temperatures (550–700 °C) and annealing times (5–600 s). Type U samples were doped in situ during growth with Si and Be to yield an $n^{++}/p^{+}/p^{++}$ structure with nominal thicknesses of the p^{+} and p^{++} layers of 700 and 300 nm, respectively. The dopant concentrations as measured by secondary ion mass spectroscopy (SIMS) were 1.5×10^{19} cm^{-3} (Si), 3.6×10^{17} cm^{-3} (Be), and 7.8×10^{18} cm^{-3} (Be) for the n^{++}, p^{+}, and p^{++} layers, respectively. The junction depths at 10^{18} cm^{-3} of the U19 and U44 samples, as measured by SIMS, were 19 and 44 nm, respectively (cf. Fig. 5).

The samples were characterized by the VDP technique and conventional Hall effect measurements on 1 cm^2 square samples and by M4PP and micro Hall effect measurements near a cleaved edge. For VDP and conventional Hall effect measurements, Ohmic contacts were formed close to each of the four sample corners by deposition of In dots on the top surface without annealing, and the magnetic flux density was 163 mT normal to the sample surface. M4PP sheet resistance measurements were performed on the CAPRES microRSP-M150 system[5] at zero magnetic flux density with an electrode pitch of 10 μm using either straight cantilevers (standard) or high aspect ratio L-shaped cantilevers (cf. Fig. 6) for sliding contact and static contact,[6] respectively. The micro Hall effect measurements were performed on a modified CAPRES microRSP-M150 system, with a nominal magnetic flux density of 500 mT normal to the sample surface, unless otherwise is stated. For micro Hall effect measurements, Au coated straight cantilever M4PPs with an electrode pitch of 20 μm were used.

IV. RESULTS

Sheet resistances of 18 different samples of types IA and IB, with different implant and annealing conditions, were measured by M4PP and VDP to correlate the two methods. M4PP measurements were performed inside the 1 cm^2 samples used for the VDP measurements and no significant R_S variations were observed. The result is summarized in Fig. 7 and shows good linear agreement of the two techniques.

To support the measurement analysis for the USJ type U samples, we performed a high resolution sheet resistance area scan of the U19 sample, which showed no sign of large R_S nonuniformities (cf. Fig. 8). For this initial test, we used L-shaped cantilevers to exclude potential mechanical surface damage of the soft InGaAs material. From the R_S measurements in Fig. 8 the measurement repeatability of M4PP can be calculated be $< 0.65\%$. Furthermore, we performed sheet resistance wafer maps, each with 361 measurement points (cf. Fig. 9). The R_S variation of the U19 sample was found to be 4.3% (relative standard deviation) with an average R_S of

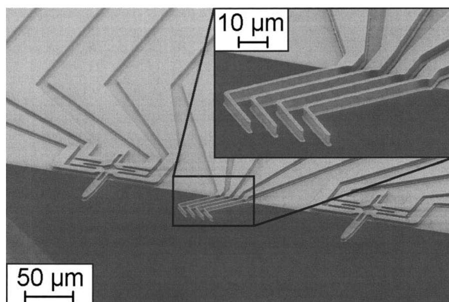

FIG. 6. M4PP with L-shaped cantilevers for static contact and strain gauge for surface detection.

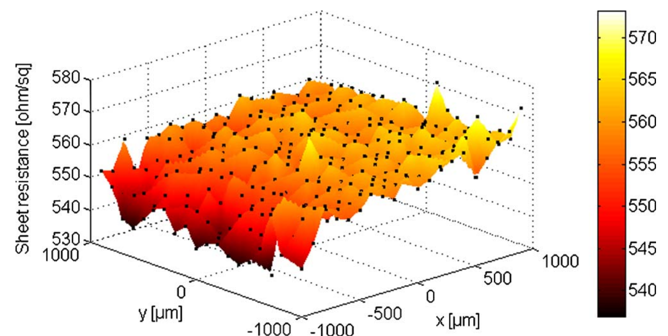

FIG. 8. (Color online) 20 × 20 points R_S area scan of the U19 sample (19 nm junction depth). The scan was performed with an L-shaped cantilever M4PP and the measurement points were measured in a random sequence.

TABLE III. Hall carrier mobility measured on the U19 sample at three different magnetic flux densities.

B_z (mT)	μ_H [cm^2/(V s)]
56.2	1675 ± 42
102	1633 ± 159
488	1974 ± 83

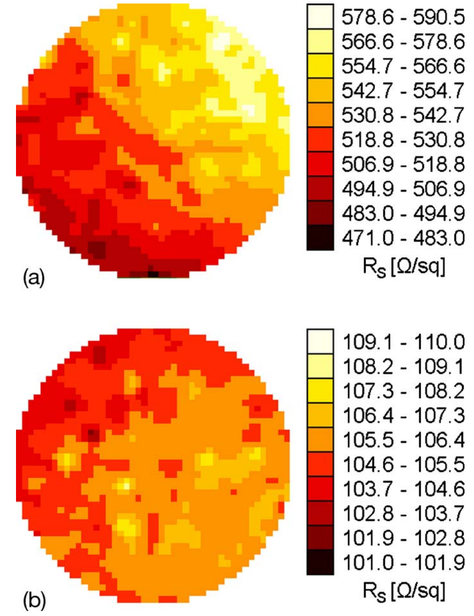

FIG. 9. (Color online) 361 points sheet resistance wafer maps of the U19 (a) and U44 (b) samples performed with standard M4PP. The average wafer sheet resistances were calculated to be 533.1 Ω/sq ± 4.3% and 105.5 Ω/sq ± 0.9%. For both measurements, the points were measured in a random sequence.

533.1 Ω/sq. The wafer map of the U44 sample was much more uniform with just 0.9% variation and with an average R_S of 105.5 Ω/sq.

Hall effect measurements were then compared for two of type IB and two type U samples. For type IB samples, the measured Hall carrier mobility was found to be 20%–25% higher using the micro Hall effect method than with the conventional Hall effect method. The micro Hall effect measurements on type U samples were repeated 51 times with relative standard deviations on R_S and μ_H of 0.6% and 3% for U44 and 0.7% and 4% for U19. In Table II, the results of the Hall effect measurements are summarized and the only obvious difference in measurement condition was the magnetic flux density.

In an attempt to explain the difference in the measured Hall carrier mobility, the magnetic field was reduced and micro Hall effect measurements confirmed a significant reduction in Hall carrier mobility when reducing the magnetic flux density (cf. Table III).

V. DISCUSSION

In this section we analyze the reliability of the two measurement techniques. For the data analysis, we shall assume a scattering factor of unity. This is in good agreement with theoretical calculations for 10^{19} cm^{-3} doped n-type InGaAs.[7]

The importance of using the modified position error suppression method as opposed to not including magnetoresistance is best evaluated at high carrier mobility and high magnetic flux density. For the U44 sample, errors of 1.5%, −6.2%, and 5.1% would have been induced on the sheet resistance, sheet carrier density, and carrier mobility, respectively, without correcting for the geometrical magnetoresistance in the position error suppression method. For the U19 sample, the errors would have been 0.9%, −4.1% and 3.3%, respectively, due to the lower carrier mobility affecting the magnetoresistance to the power of 2.

On the IA and IB samples, VDP measured, on average, 3.4% lower R_S than M4PP. It is well known that positioning of electrical contacts near the corners of a square sample is critical for precise sheet resistance measurements when using VDP. A geometrically induced measurement error of −3.4% will result when the four contacts are placed on the diagonals of an $L \times L$ square at a distance of roughly $0.25 \times L$ from the corners.[8] However, such a large position error does not appear to be a general trend for the measured samples. For the M4PP measurements, we first notice that the measured sheet resistance is independent of the use of sliding contact or static contact. Also, the repeatability was found to be $< 0.65\%$ on the U19 sample which shows the largest sample variation. This is in good agreement with previous results, which showed a repeatability and reproducibility of M4PP measurements on Si USJ to be $< 0.1\%$.[9] The average differ-

TABLE II. Comparison of Hall effect measurements performed with conventional Hall effect method and micro Hall effect method on four different samples.

	Hall effect–square sample				Micro Hall effect			
Sample name	B_z (mT)	R_0 (Ω/sq)	N_{HS} (10^{13} cm^{-2})	μ_H [cm^2/(V s)]	B_z (mT)	R_0 (Ω/sq)	N_{HS} (10^{13} cm^{-2})	μ_H [cm^2/(V s)]
IB1 (600 °C, 60 s)	163	44.0	7.34	1931	500	44.55	6.03	2323 ± 62
IB2 (600 °C, 600 s)	163	42.4	7.70	1911	500	43.36	5.99	2402 ± 21
U19	163	363	1.33	1288	488	556.8	0.588	1974 ± 83
U44	163	95.1	3.72	1770	488	106.3	2.37	2473 ± 73

ence of 3.4% between the two measurement techniques is, however, not necessarily an inherent measurement error but could be attributed to calibration errors such as different resistance reference, temperature difference, or time between measurements.

Although conventional Hall effect and micro Hall effect methods measure the same sheet resistance on type IB sample, the Hall sheet carrier density and Hall carrier mobility clearly differs by 20%–25%. However, a difference of ~16% between micro Hall effect measurements at 500 mT and 50–100 mT is also seen (cf. Table III), which indicates a dependency on the magnetic flux density and could be the result of a change in the Hall scattering factor. For both methods, the sheet carrier density measured for the ion implanted IB1 and IB2 samples is only 6%–8% of the implanted dose (10^{15} cm^{-2}). However, this is in very good agreement with the results previously obtained by Penna *et al.*[10] In the light of these results, we assume that both methods do, in fact, measure Hall effect correctly on type IB sample.

On the USJ type U samples, we see a clear difference in the measured sheet resistance for VDP and M4PP. We note that the VDP measurements were performed on two structures of each sample, and that the results were reproduced within expected experimental uncertainty; also the results were independent of the measurement current. Likewise, the M4PP measurements were reproducible and independent of the measurement current as well as electrode pitch. From our previous work with p^{++}/n^{+} Si USJ,[1] we know that high leakage current leads to a reduced measured sheet resistance. Such explanation fits well with the results of the U44 and U19 samples, for which a reduced R_S of 11% and 35% is seen for the 44 and 19 nm films, respectively, as compared to M4PP. At this time the origin of leakage current is unknown; i.e., leakage current can occur either beneath the In contacts or as a general n^{++}/p^{+} junction leakage as described in Ref. 11.

Leakage current will also reduce the measured Hall sheet resistance R_H, which results in an apparent increase in Hall sheet carrier density as they are inversely proportional; we recall that $N_{HS}=ZB_z/(eR_H)$. The Hall carrier mobility depends both on the measured R_S and R_H ($\mu_H=R_H/(ZB_zR_0)$) and thus in the presence of leakage current, the calculated mobility will also be incorrect, although the error cancels out to some unknown extent.[12]

To complete the analysis of measurement reliability, we note that whereas M4PP R_S measurements were straightforward, a higher than normal standard deviation in measurement repeatability was observed for U19 ($<0.65\%$) as compared to normally $<0.1\%$ for Si USJ.[9] However, the increase in measurement standard deviation for the U19 sample could be related to the extremely low sheet carrier density (cf. Table II) and carrier fluctuations. For instance, if we assume a box profile with the carrier concentration of $n=1.5\times10^{19}$ cm^{-3} as found by SIMS; then the average number of carriers N within a cube of dimensions d^3 will be on the order of $N=nd^3=n_Sd^2=n_S^3/n^2\approx1$, where d is defined by the electrical junction depth and n_S is the sheet carrier density. Thus, the average number of carriers in a cube is so low that it can result in discontinuities of the conductive n^{++} surface layer,[13] which may affect measurement repeatability.

The carrier mobility measured for the most shallow junction, U19, is 18% lower compared to the average of the U44, IB1, and IB2 samples. This could be the result of increased surface scattering, i.e., the electron mean free path approaches the conductive layer thickness. The electron mean free path may be estimated as $\lambda=\mu v_{\text{th}}m^*/e\approx6$ nm, where v_{th} is the thermal carrier velocity, m^* is the effective electron mass, e is the unit charge, and the carrier mobility measured for the U44 sample is used. In addition, the effective layer thickness is expected to be less than the metallurgical junction depth of 19 nm due to surface and junction depletion layers; thus, increased surface scattering seems to agree with the experimental results. Another possible reason is that lateral continuity may be lost in some areas due to the low sheet carrier density and carrier fluctuations. The latter agrees with the above analysis on carriers in a box.

VI. CONCLUSION

For sheet resistance characterization of InGaAs, we established a sensible linear agreement between conventional VDP measurements and M4PP measurements on n^{++}/insulating structures. However, for ultra-shallow n^{++}/p^{+} structures with junction depths of 44 and 19 nm, we find M4PP much more reliable. A significant leakage current is proposed to be the reason for the lower sheet resistance measured with VDP, which, in turn, also prevents accurate Hall effect measurements on USJ.

For micro Hall effect measurements, we have derived an approximation to the position error suppression method in order to include geometrical magnetoresistance, which is important for $(\mu_HB_z)^2\geqslant0.01$. With the micro Hall effect method, we observed a difference of ~16% between Hall carrier mobilities measured at low magnetic flux density (56 and 102 mT) and at moderate magnetic flux density (488 mT). Except for this difference, a good correlation between conventional Hall effect and micro Hall effect was found on n^{++}/insulating structures. For USJ n^{++}/p^{+} structures, micro Hall effect showed repeatabilities of 3% and 4% on carrier mobility for 44 nm and 19 nm junction depths, respectively. Finally, we observed an ~18% decrease in the carrier mobility for the 19 nm USJ as compared to the 44 nm junction. We expect this may be a scaling effect caused by increased surface scattering or lost continuity in some areas due to low sheet carrier density and carrier fluctuations.

[1] T. Clarysse *et al.*, Mater. Res. Soc. Symp. Proc. **912**, 197 (2006).
[2] D. H. Petersen, O. Hansen, R. Lin, and P. F. Nielsen, J. Appl. Phys. **104**, 013710 (2008).
[3] D. H. Petersen, O. Hansen, R. Lin, P. F. Nielsen, T. Clarysse, J. Goossens, E. Rosseel, and W. Vandervorst, *Proceedings of the 16th IEEE International Conference on Advanced Thermal Processing of Semiconductors, RTP 2008* (IEEE, New York, 2008), pp. 251–256.
[4] R. S. Popović, *Hall Effect Devices, Magnetic Sensors and Characterization of Semiconductors*, The Adam Hilger Series on Sensors (Adam Hilger, Bristol, 1991).

[5]Capres A/S, http://www.capres.com.
[6]D. H. Petersen, O. Hansen, T. M. Hansen, P. R. E. Petersen, and P. Bøggild, Microelectron. Eng. **85**, 1092 (2008).
[7]Y. Takeda and M. A. Littlejohn, Appl. Phys. Lett. **40**, 251 (1982).
[8]D. W. Koon, A. A. Bahl, and E. O. Duncan, Rev. Sci. Instrum. **60**, 275 (1989).
[9]D. Kjaer, R. Lin, D. H. Petersen, P. M. Kopalidis, R. Eddy, D. A. Walker, W. F. Egelhoff, and L. Pickert, AIP Conf. Proc. **1066**, 167 (2008).
[10]T. Penna, B. Tell, A. S. H. Liao, T. J. Bridges, and G. Burkhardt, J. Appl. Phys. **57**, 351 (1985).
[11]C. L. Petersen, R. Lin, D. H. Petersen, and P. F. Nielsen, *Proceedings of the 14th IEEE International Conference on Advanced Thermal Processing of Semiconductors, RTP 2006* (IEEE, New York, 2006), pp. 153–158.
[12]T. Clarysse *et al.*, Mater. Sci. Eng., B **154–155**, 24 (2008).
[13]D. H. Petersen *et al.*, J. Vac. Sci. Technol. B **28**, C1C27 (2010).